Spectrochimica Acta Part A: Molecular and Biomolecular Spectroscopy 348 (2026) 127107

Contents lists available at ScienceDirect

Spectrochimica Acta Part A:
Molecular and Biomolecular Spectroscopy

journal homepage: www.journals.elsevier.com/spectrochimica-acta-part-a-molecular-and-biomolecular-spectroscopy

Reliability analysis of photoluminescence measurement data from the intrinsic limitation on the instrument to the practical limitations during the experiments

Meirong Liu [a,b,*], Hongxia Sun [a], Shasha Li [a,b], Rongjuan Feng [a,b], Jiao Mu [a,b]

[a] Beijing National Laboratory for Molecular Sciences (BNLMS), Institute of Chemistry Chinese Academy of Sciences, Beijing 100190, PR China
[b] Center for Physicochemical Analysis and Measurement, Institute of Chemistry Chinese Academy of Sciences, Beijing 100190, PR China

HIGHLIGHTS

- Grating performance at the excitation site can result in some fluorescence artifacts. This can be resolved by optimizing the excitation light wavelength or silt size.
- Distortion of the temporal decay profiles induced by the secondary reflected laser can be avoided by precise control of the laser's incident angle or sample orientation.
- Excessively strong scattering light will lead to stray light across a broad range through the grating multi-stage diffraction.

GRAPHICAL ABSTRACT

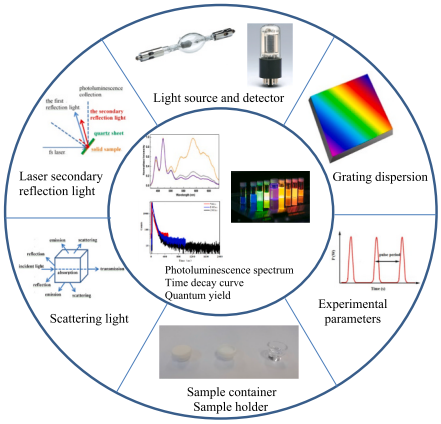

ARTICLE INFO

Keywords:
Photoluminescence reliability
Spectrometer grating
Quantum yield
Decay kinetics
Secondary reflection artifacts
Time-resolved spectroscopy

ABSTRACT

Photoluminescence spectroscopy serves as a fundamental characterization technique widely employed in chemistry and materials science research. The reliability of the original data is crucial, as it directly determines the scientific conclusions obtained based on data processing and analysis. This work presents a systematic investigation of factors influencing photoluminescence data reliability through comprehensive analysis of the complete optical pathway, including the instrument intrinsic limitations and practical experimental limitations. Key findings reveal that instrument grating performance at the excitation site can lead to the introduction of some stray light within the range of 350 nm–500 nm at excitation wavelengths below 300 nm, thereby resulting in photoluminescence artifacts in certain sample analyses. These artifacts can be addressed through optimization of the excitation light wavelength and adjustment of the excitation/emission silt dimensions. The practical limitations during the experiments, such as the interaction of the excitation light with the sample including the scattering light, sample container, and the secondary reflected light of the laser, can all influence the data

* Corresponding author at: Beijing National Laboratory for Molecular Sciences (BNLMS), Institute of Chemistry Chinese Academy of Sciences, Beijing 100190, PR China.
E-mail address: mrliu@iccas.ac.cn (M. Liu).

https://doi.org/10.1016/j.saa.2025.127107
Received 26 July 2025; Received in revised form 25 September 2025; Accepted 27 October 2025
Available online 31 October 2025

reliability. Notably, the secondary reflected light of the laser under ultrafast measurement conditions may distort temporal decay profiles, requiring precise control of the laser's incident angle or sample orientation. Excessively strong scattering light will lead to the presence of stray light across a broad range of the emission spectrum through the grating multi-stage diffraction. By implementing the proposed methodologies, researchers can substantially improve the accuracy and reproducibility of photoluminescence data. This work provides a practical framework for acquiring reliable photoluminescence spectra and decay kinetics across diverse material systems.

1. Introduction

Photoluminescence is the newly generated light, produced by the excitation light to excite the sample. This technique offers high analytical sensitivity, enabling the detection of target substances at low concentrations. Additionally, it exhibits strong selectivity, allowing for the differentiation of various analytes through both steady-state and transient photoluminescence spectra.

Similar to photoluminescence, Raman scattering also involves newly generated light. However, Raman measurements typically employ highly monochromatic lasers, characterized by a line width of no more than 1/20 of the nominal resolution [1]. Raman spectrometers are generally equipped with multiple lasers, and each equipped with an edge filter with an optical density (OD) of more than 6. For Raman shift above 100 cm^{-1}, stray light interference is generally negligible. In contrast, the excitation wavelength of photoluminescence samples is various, often relying on continuous light source such as xenon lamps in conventional photoluminescence measurements. Even after passing through a monochromator, the excitation light still retains a relatively wide wavelength range, leading to significant stray light effects. Furthermore, photoluminescence has a longer lifetime than Raman scattering and is more susceptible to environmental factors. As a result, photoluminescence measurements are inherently more complex than Raman spectroscopy, necessitating careful evaluation of the data to ensure they accurately reflect sample properties.

According to the ACS database, approximately 40 % of the literature published in 2024 involves photoluminescence data, and the application of photoluminescence data in the fields of chemistry, materials, and biology is exceedingly prevalent. If the reliability of the photoluminescence data cannot be guaranteed, some important inferences will not be available. For example, photoluminescence experiments combined with theoretical calculations have revealed inverted T_1 and S_1 energy levels in certain molecules, resulting in a small negative ΔE_{ST} and a short delayed photoluminescence lifetime of 0.2 μs [2]. Without accurate data, this particular phenomenon will not be found. Similarly, photoluminescence analysis of Martian craters has identified aggregates of organic minerals, suggesting the prevalence of aromatic small molecules on Mars [3]. Errors in peak position, intensity, or shape could cast doubt on these findings, undermining significant scientific conclusions.

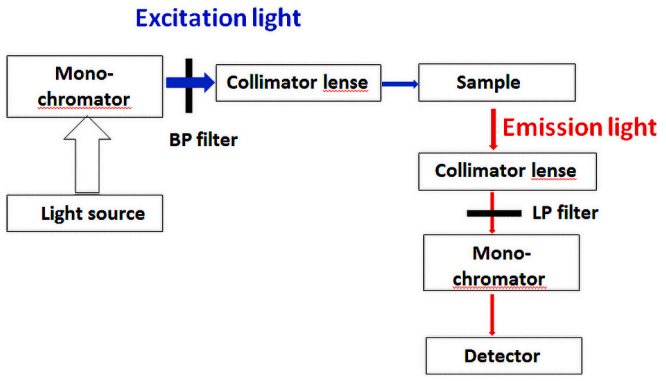

Fig. 1. Schematic diagram of the optical path in a conventional commercial photoluminescence spectrometer. BP denotes bandpass filter and LP represents longpass filter.

Fig. 1 illustrates a typical photoluminescence spectrometer setup. Excitation light from the light source passes through a monochromator and collimator lenses, subsequently interacting with the sample. The sample absorbs the excitation light and produces photoluminescence, and the resulting photoluminescence then collected via another collimator lenses and monochromator, ultimately reaching the detector. It can be seen that key factors influencing data reliability include the light source, monochromator, collimator lenses, the interaction of the excitation light with the sample, the detector, etc. The light source can be a continuous light source (e.g., xenon lamp) or monochromatic light (e.g., laser). When using a laser as the light source, a monochromator is typically not employed. The monochromator is generally constituted of a grating or prism. Because the grating spectrophotometer has a high resolution and short optical path, contemporary photoluminescence spectrometers predominantly incorporate grating as monochromators. The collimator lenses can be a convex lens or a concave mirror. The convex lens has a simple focusing light path but introduce chromatic aberration. In contrast, the concave mirror focusing optical path is relatively complex and has little aberration, each with its own advantages. There are different types of detectors. The detectors required for steady-state photoluminescence and transient photoluminescence are different, but they are generally photoelectric detectors with high sensitivity. Because the scattered light from the sample is minimal at an angle of 90^o to the excitation light [4], commercial photoluminescence spectrometers typically employ 90^o detection geometry.

Photoluminescence measurements are subject to numerous intrinsic limitations on the instrument and the practical limitations during the experiments, including light sources, detectors, grating, interaction of the excitation light and the sample, and the experimental parameters. These can all affect the data reliability. At present, existing literature on photoluminescence data accuracy primarily focuses on specific sample systems [5–9], novel detection techniques [10–15], and innovative data processing methods [16]. Under ultrafast measurement, photoluminescence temporal evolution artifact was observed. This phenomenon was attributed to the fact that the photoluminescence penetrates through the sample and is reflected by the back surface and creates a second rise in the photoluminescence temporal evolution [17].

However, systematic studies addressing the reliability of raw data remain scarce. Inaccurate raw data - whether due to instrumental artifacts or experimental conditions – can compromise subsequent analyses, including steady-state spectra, decay curves, and quantum yield calculations. Without ensuring the reliability of raw data, derived scientific conclusions may be untenable. To address this gap, this paper comprehensively examines the factors affecting the reliability of photoluminescence data from the intrinsic limitation on the instrument to the practical limitations during the experiments.

In this investigation, it was demonstrated that the grating at the excitation site can produce stray light spanning 350–500 nm when excitation wavelengths below 300 nm are employed, resulting in artifactual photoluminescence signal in some samples. These artifacts may be effectively suppressed through optimization of the excitation wavelength and appropriate adjustment of the excitation and emission slit widths.

Several practical experimental factors—including interactions between the excitation light and the sample, such as scattering, container

effects, and secondary laser reflections—may also compromise data accuracy. Notably, under ultrafast measurement conditions, laser secondary reflections from the rear surface of the optical elements can significantly distort temporal decay profiles. Such distortions can be alleviated by controlling the laser incident angle or modifying the sample orientation. Furthermore, excessively strong scattering light will lead to the presence of stray light across a broad range of the emission spectrum through the grating multi-stage diffraction. The incorporation of band-pass or long-pass filters substantially attenuates this effect, acquiring reliable data.

The methodologies proposed in this work facilitate markedly improved accuracy and reproducibility in photoluminescence spectroscopy. Our findings provide a practical and systematic framework for the acquisition of reliable photoluminescence spectra and decay kinetics across diverse material systems.

2. Methods and materials

Steady-state and time-resolved photoluminescence measurements were performed using an Edinburgh Instruments FLS980 photoluminescence spectrometer (Edinburgh, UK) equipped with built-in long-pass filters (420 nm and 670 nm). For ultrafast measurements, a Astrella-Opera Solo femtosecond ultrafast spectrometer (Coherent Inc., USA) was employed to characterize laser secondary reflection artifacts. Femtosecond ultrafast spectrometer was composed of a regenerative-amplified Ti: sapphire laser system (Coherent Astrella) and a streak camera. The regenerative-amplified Ti: sapphire laser system (Legend Elite USX, center wavelength of 800 nm, pulse duration of 35 fs, pulse energy of 7 mJ, repetition rate of 1 kHz) was seeded with a mode-locked Ti: sapphire laser system (Vitara S). The output 800 nm fundamental of the amplifier was split into two beam pulses. The main part of the fundamental beam went through the optical parametric amplifiers (Opera solo), whose output light was set as the pump laser with a wavelength of 240–2400 nm. Streak camera was used as the detector and the time resolution for the femtosecond ultrafast spectrometer is 2 ps.

The bandpass (BP) filters utilized in this study were sourced from ChromA (United States), and the longpass (LP) filters were acquired from Hengyang Optics (China) and Thorlabs (United States). Mirror (UV-Enhanced Aluminum, $R_{avg} > 90$ % from 250 to 450 nm) was purchased from Thorlabs (United States). Solid pyrene (98 % , reagent grade) was acquired from J&K Scientific (China). Rhodamine B was purchased from the Beijing BioLab Technology Co., Ltd. (China), and was dissolved in anhydrous ethanol at a concentration of 5×10^{-5} M. The dye-polymer melt was fabricated by the research team.

3. Results and discussion

3.1. Light source and detector

For the photoluminescence spectrometer, the wavelength dependence of components such as the light source, detector, grating, and collimator lenses are corrected with designated correction files. However, near the spectral detection limits, these correction algorithms frequently misidentify some noise as a signal, leading to instances of overcorrection. To ensure data fidelity, we recommend: (1) comparing corrected spectra with corresponding raw data, and (2) when anomalies are observed, verifying measurements using an alternative spectrometer whose operational wavelength range better matches the spectral features of interest. This validation protocol significantly enhances result reliability, particularly for emission signals approaching the instrument's detection boundaries.

3.2. Monochromator

Commercial photoluminescence spectrometers typically employ grating-based monochromator to disperse broadband radiation from xenon light sources into discrete wavelengths. However, the intrinsic limitations of grating-based monochromators can lead to significant artifacts and measurement uncertainties, particularly in the regime of short-wavelength excitation. This section presents a comprehensive investigation of the artifacts induced by the monochromator.

Through the systematic investigation of the monochromator performance, significant artifacts were observed even under seemingly ideal conditions. When only the solution sample holder was mounted in the sample chamber (without cuvettes or quartz sheets), a significant signal was detected at short excitation wavelengths, particularly when large emission slits were employed. In this case, almost all the excitation light penetrates the solution sample holder and is absorbed by the blackened interior wall of the sample chamber. As demonstrated in Fig. 2a, the observed signal originates from the interaction of the excitation light and the inner wall of the sample chamber, potentially through diffuse reflection or other mechanisms. This phenomenon constitutes a photoluminescence artifact that necessitates meticulous consideration during experimental design and data interpretation. These findings establish an important reference for instrument blank measurement in PL spectroscopy.

As shown in Fig. 2a, significant stray light signals (>2000 a.u.) were observed in the 350–500 nm range using a 250 nm excitation wavelength. These artifacts exhibited pronounced wavelength dependence, with their intensity progressively diminishing as the excitation wavelength increased. Notably, stray light signals became negligible at excitation wavelength above 310 nm, suggesting a critical threshold for reliable measurements. For weakly fluorescent samples, it is advised to mitigate the influence of photoluminescence artifacts by careful design of blank control experiments or by optimization of acquisition parameters (including excitation wavelength selection and slit width adjustment). Fig. 2b outlines the experimental parameters, encompassing an excitation wavelength (250–334 nm), an excitation bandwidth of 8 nm, and an emission bandwidth of 4 nm. A bandpass (BP) filter was added at the excitation site.

The stray light observed within the 350–500 nm range in Fig. 2a may be caused by impure excitation light after monochromator splitting. To verify this hypothesis, a mirror was positioned at the site where the solid sample is placed on the solid sample holder to reflect a portion of the excitation light directly into the detector, enabling spectral analysis of the excitation light. How is the monochromaticity of the excitation light after the xenon light source is split by the grating? How is the spectral distribution of the excitation light? Fig. 3a, c, e, g, and i present the reflected excitation light spectra (REL) after the grating splitting at 250 nm, 270 nm, 292 nm, 310 nm, and 334 nm, both with and without a BP filter. For comparison, Fig. 3b, d, f, h, j, and k overlay the REL spectra with the instrument blank spectra and provide details on experimental parameters. To ensure precise REL spectra analysis and avoid detector saturation, a smaller slit width was used compared to that in Fig. 2b.

REL spectra indicate that the excitation light from the monochromator is not perfectly monochromatic, exhibiting a broad spectral distribution, especially at shorter wavelengths (250 nm and 270 nm). At these excitation wavelengths, significant stray light in REL appears within the 350–450 nm range, closely matching the instrument blank signal in Fig. 2a. This correlation confirms that the spurious signals within the 350–500 nm range originate from the excitation light. As the excitation wavelength increases (292 nm, 310 nm, and 334 nm), the REL intensity within the 400–500 nm range becomes negligible. However, the instrument blank spectrum continues to display broad emission within the 400–500 nm range, suggesting that the residual signal may arise from the interaction between the excitation light and the inner wall of the sample chamber.

When a BP filter is applied at the excitation site, both the excitation light intensity and the stray light intensity (350–450 nm) are substantially reduced, significantly improving the monochromaticity of the excitation light. This finding highlights the importance of using optical

a

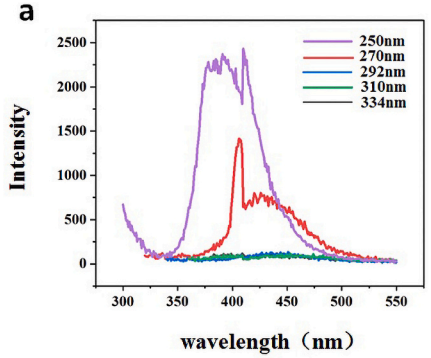

b

λ_{ex}(nm)	excitation BW (nm)	emission BW (nm)	BP filter (nm) /BW (nm)	acquisition starting wavelength（nm）
250	8	4	250\20	300
270	8	4	270\15	320
292	8	4	292\10	340
310	8	4	310\10	360
334	8	4	334\10	380

Fig. 2. a Instrument blank signals measured at various excitation wavelengths. **b** Corresponding acquisition parameters for different excitation wavelengths, BW denotes bandwidth.

filters to enhance spectral purity and minimize stray light interference in PL measurements.

The data demonstrate that stray light within the 350–500 nm range can severely compromise the reliability of PL measurements, particularly for weakly fluorescent samples. The stray light (350–500 nm) may be misinterpreted as sample emission, leading to erroneous conclusions about the sample's optical and electronic properties. To mitigate these effects, the following strategies are recommended:

1. **Incorporation of BP Filters:** As demonstrated in the experiments, employing a BP filter at the excitation site effectively narrows the wavelength range of the excitation light and reduces stray light intensity in the emission spectrum. However, it should be noted that this approach concurrently diminishes the excitation light intensity, potentially limiting its applicability for weakly fluorescent samples.
2. **Implementation of Instrument Blank Experiments:** Instrument blank experiments can be strategically designed to isolate and quantify the contribution of stray light to the measured photoluminescence (PL) spectra. By systematically comparing sample spectra with instrument blank spectra, the influence of stray light can be accurately assessed and corrected.
3. **Optimization of Acquisition Parameters:** Fine-tuning acquisition parameters, such as excitation wavelength and slit size, can significantly minimize stray light interference in PL spectra. Specifically, narrower emission slits effectively attenuate stray light effects. However, this adjustment may concurrently reduce the signal-to-noise ratio (SNR) of the measurements, necessitating careful optimization based on specific experimental conditions. Notably, when the excitation wavelength exceeds 300 nm, the impact of stray light on PL spectra becomes negligible.

3.3. Interaction of the excitation light with the sample

3.3.1. Effect of the scattered light

A sample absorbs the excitation light, producing photoluminescence, which is about $1/10^6$ of the excitation light intensity. But a portion of the excitation light also may directly reach the detector, which constitutes the undesired signal. In the PL optical configuration illustrated in Fig. 1, for dilute solutions or optically transparent thin film materials, almost all excitation light penetrates the sample, with minimal scattered light entering the detector in the right-angle collection geometry. In contrast, for concentrated solutions, solid powders, or bulk solid samples, although the excitation light is scattered least at the right-angle direction, the contribution of scattered light can still dominate over the photoluminescence signal. In some cases, the scattered light intensity may exceed the photoluminescence intensity by several orders of magnitude. The intensity of the scattered light is directly proportional to the sixth power of the particle size and inversely proportional to the fourth power of the wavelength [4]. Effective suppression of scattered light is critical for obtaining accurate and reliable photoluminescence measurements.

When a sample exhibits strong scattering, the scattered excitation light interacts with the grating at the emission site through multi-order diffraction at various angles. Given that the excitation light inherently covers a specific wavelength range (about 30 nm , after BP filtering), this multi-order diffraction at different angles generates stray light across a broad spectral range [18,19]. This stray light overlaps with the target photoluminescence signal and severely compromises its detection. Even when the acquisition starting wavelength is set far from the excitation wavelength, this interact introduces stray light across a broad range of the emission spectrum (Fig. 4a, b), leading to significant distortion of the photoluminescence spectrum. For the Ru_1/TiO_2 nanosheets, the intensity of the scattered light substantially surpasses the photoluminescence intensity, severely compromising the reliability of the photoluminescence data.

In Fig. 4a, the excitation wavelength was set to 370 nm, with a 370 nm BP (BW 15 nm) filter at the excitation site and a 400 nm LP filter at the emission site. Despite these measures, the acquired emission spectrum remained entirely distorted (red line). The abrupt spectral change observed near 670 nm arises from the instrument's built-in 670 nm LP filter. However, when an additional 420 nm LP filter was incorporated at the emission site, the authentic emission spectrum was successfully acquired (black line).

The implementation of dual LP filters at the emission site effectively minimizes the excitation light entering the monochromator, thereby suppressing the interaction between the excitation light and the grating at the emission site. This approach successfully eliminates the generation of broadband stray light in the emission spectrum.

This confirms that the stray light across the broad wavelength range is originated from the excitation light. Since the excitation light exhibits a bandwidth of approximately 30 nm, the stray light across such a wide wavelength range must indeed be produced by multi-order diffraction of the excitation light with the grating at different angles.

For samples exhibiting strong scattering, the excitation light can be purified by employing a bandpass (BP) filter at the excitation site, while longpass (LP) filters at the emission site effectively suppress stray light interference. In cases where suitable filters are unavailable, an alternative approach involves grinding the sample and dispersing it in a KBr matrix to mitigate scattering effects. However, mechanical grinding may alter the intrinsic photoluminescence properties of the sample and should be used with caution.

Notably, BP and LP filters primarily attenuate Rayleigh scattering. In contrast, the wavelength of Raman scattering is different from that of excitation light and occurs with photoluminescence, rendering it unresolvable through conventional filtering. Raman peaks can be distinguished from PL signals by their excitation-wavelength-dependent shift, whereas PL peaks remain invariant. Furthermore, time-resolved spectroscopy offers a robust means of discrimination, as Rayleigh and Raman

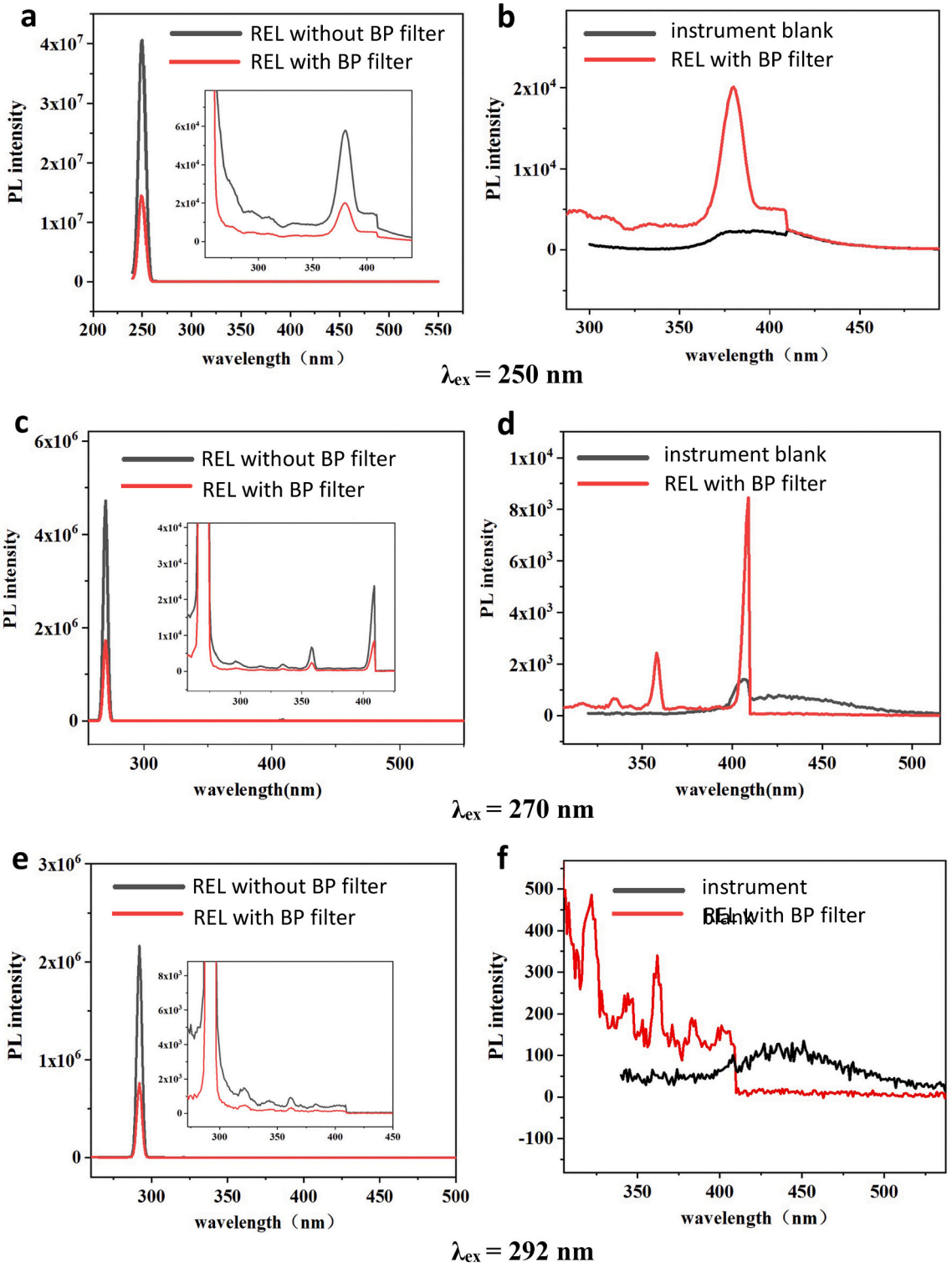

Fig. 3. Spectral analysis of reflected excitation light (REL) after grating dispersion, with the excitation wavelengths of 250 nm **a**, 270 nm **c**, 292 nm **e**, 310 nm **g**, 334 nm **I**, and the enlarged image in the inset. Comparison of REL spectra and instrument blank spectrum, with the excitation wavelengths of 250 nm **b**, 270 nm **d**, 292 nm **f**, 310 nm **h**, and 334 nm **j**. Experimental parameters as shown in **k**.

scattering exhibit picosecond-scale lifetimes, while PL typically occurs on the nanosecond timescale.

3.3.2. *Sample container or sample holder*

3.3.2.1. Sample container. In quantum yield measurements of solid samples, a PTFE whiteboard is commonly employed as a reference blank, with the sample typically loaded into a PTFE sample container as illustrated in Fig. 5. However, this approach introduces systematic errors due to the non-negligible light absorption by the PTFE whiteboard or PTFE sample cantainer, particularly in the ultraviolet spectral region.

We evaluated the light absorption of PTFE whiteboards, PTFE solid

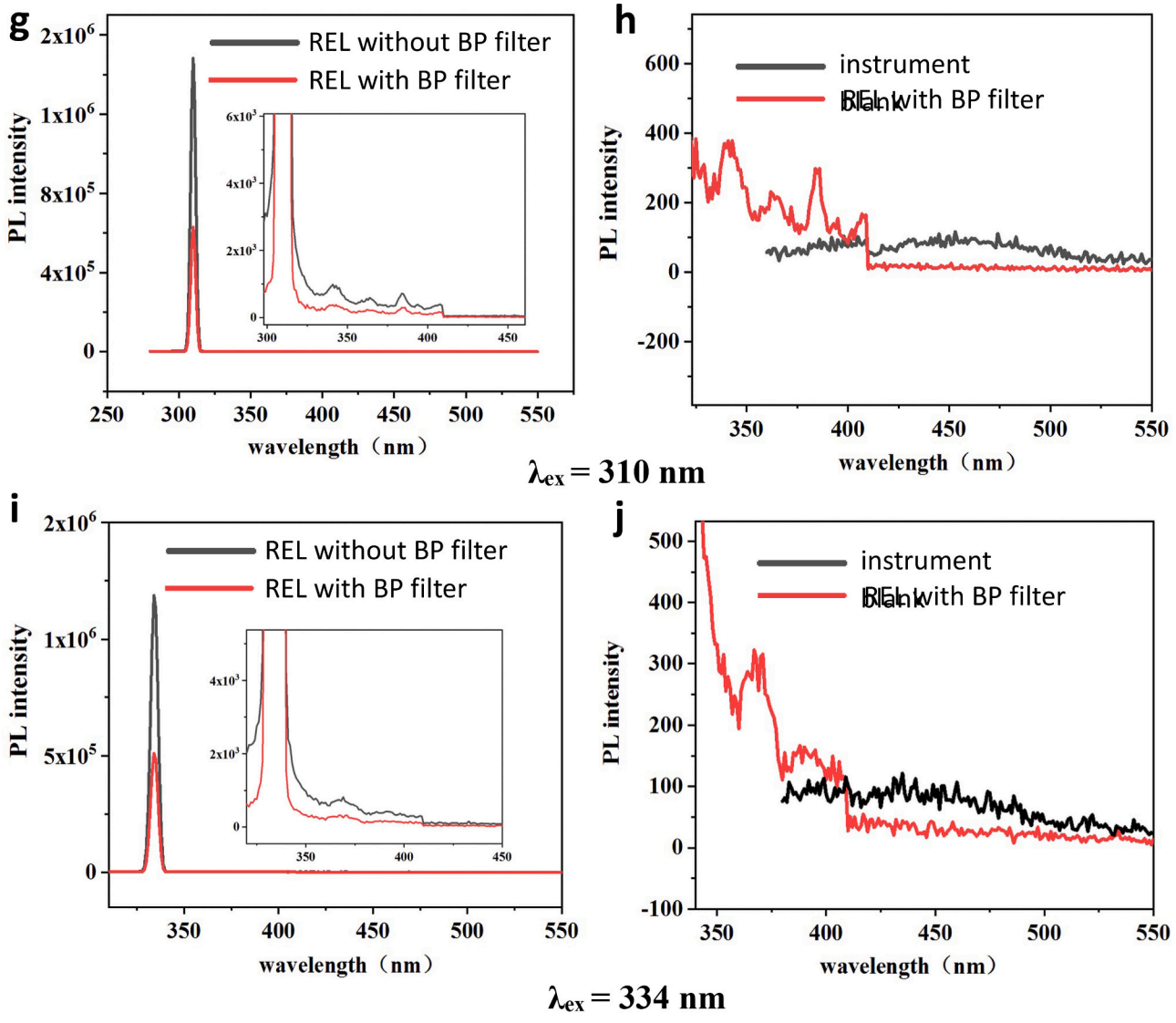

k

λ_{ex}(nm)	(REL) excitation BW (nm)	(REL) emission BW (nm)	(instrument blank) excitation BW (nm)	(instrument blank) emission BW(nm)	BP filter (nm) /BW (nm)
250	7.5	4.0	8.0	4.0	250\20
270	3.0	3.0	8.0	4.0	270\15
292	3.0	3.0	8.0	4.0	292\10
310	3.0	3.0	8.0	4.0	310\10
334	3.0	3.0	8.0	4.0	334\10

Fig. 3. (*continued*).

sample container, and quartz solid sample container across various excitation wavelengths (Table 1). The number of absorbed photons was found to be similar between the PTFE solid sample container and the PTFE whiteboard. Compared to the quartz solid sample container, the number of absorbed photons for the PTFE solid sample container is substantially higher, which decreases with the increase of the excitation wavelength.

When using either the PTFE whiteboard or empty sample container as a blank reference, the subsequent placement of the solid sample in the container inevitably blocks a portion of the PTFE surface. Consequently, the measured absorption of the sample-loaded container becomes artificially lower than that of the blank reference. This leads to an

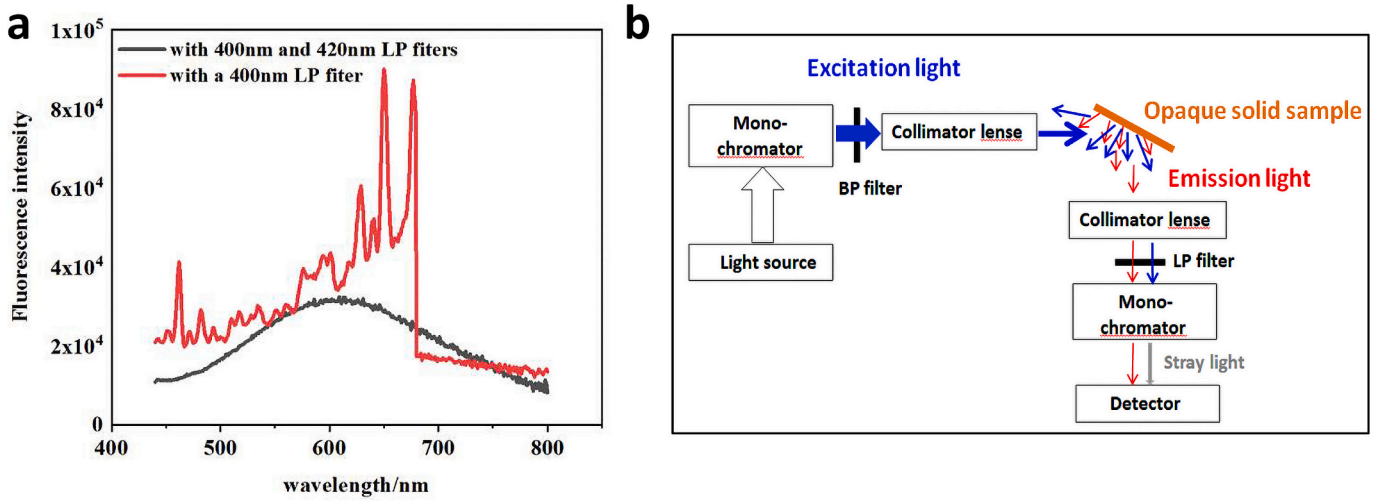

Fig. 4. **a** Photoluminescence (PL) emission spectra of Ru_1/TiO_2 nanosheets, acquired with a 370 nm BP (BW 15 nm)filter at the excitation site. The red and black lines represent the spectra obtained with a single 400 nm LP filter and dual LP filters (400 nm and 420 nm) at the emission site, respectively. **b** Schematic illustration of the scattered light path in a commercial PL spectrometer when measuring an opaque solid sample. (For interpretation of the references to colour in this figure legend, the reader is referred to the web version of this article.)

Fig. 5. The PTFE whiteboard (left), the PTFE solid sample container (middle), and the quartz solid sample container (right).

Table 1
Analysis of photon loss for PTFE whiteboard and different types of solid sample container.

λ_{ex}(nm)	λ_{em}(nm)	excitation BW (nm)	emission BW (nm)	NO* (N.P.)	PTFE whiteboard (N.P./ PLP)	PTFE solid sample container (N.P./ PLP)	quartz solid sample container (N.P./ PLP)
250	250	15.0	3.0	41	27/34.1 %	24/41.5 %	33/19.5 %
270	270	8.0	1.0	97	61/37.1 %	58/40.2 %	85/12.4 %
290	290	6.0	0.6	98	65/33.7 %	63/35.7 %	91/7.1 %
310	310	4.2	0.42	94	67/28.7 %	66/29.8 %	88/6.3 %
330	330	3.4	0.34	98	72/26.5 %	72/26.5 %	94/4.1 %
350	350	3.0	0.30	98	73/25.5 %	74/24.5 %	93/5.1 %
370	370	2.0	0.25	94	72/23.4 %	73/22.3 %	91/5.2 %
390	390	2.2	0.22	93	72/22.6 %	74/20.4 %	89/4.3 %
410	410	2.1	0.21	97	84/13.4 %	87/10.3 %	95/2.0 %
430	430	2.0	0.18	97	89/8.2 %	91/6.2 %	96/1.0 %
450	450	1.8	0.17	97	91/6.2 %	92/5.1 %	96/1.0 %

NO* indicates the number of photons detected when neither the PTFE whiteboard and the PTFE solid sample container, nor any other sample container is placed inside the integrating sphere. Columns 6 to 8 show the number of photons detected and the corresponding photon loss percentage—compared to the value in column 5—after placing the PTFE whiteboard, the PTFE solid sample container, or the quartz solid sample container into the integrating sphere. (PTFE: polytetrafluoroethylene, N.P.: number of photons, PLP: photon loss percentage. The unit for the number of photons is ten thousand).

underestimation of the actual photons absorbed by the sample, resulting in a systematically overestimated quantum yield value. The magnitude of this error depends on multiple factors including excitation wavelength, sample quantity, absorption coefficient, and the sample's intrinsic quantum yield.

To minimize these measurement artifacts and obtain more reliable quantum yield values, we recommend replacing PTFE sample container with quartz counterparts. Quartz demonstrates significantly lower optical absorption compared to PTFE across the 250–400 nm spectral range, thereby substantially reducing measurement errors associated with container absorption.

The quantum yields (QYs) of opaque solid pyrene and a dye-polymer melt were also measured employing two different solid sample containers. The measurements revealed that the QYs were consistently higher when a PTFE container was used, compared to a quartz container. Comprehensive details of these experiments are available in the

Supplementary Material.

For the accurate determination of absolute quantum yield, meticulous cleaning of the integrating sphere is essential to ensure blank measurements exhibit no photoluminescence background. Particular attention must be paid to samples exhibiting spectral overlap between their excitation and emission bands, as this can lead to secondary excitation effects during conventional quantum yield measurements, resulting in a higher quantum yield value. In this case, indirect measurement can be employed [20].

3.3.2.2. Solid sample holders. Solid sample holders are essential for conducting photoluminescence experiments on solid powder samples, membrane samples, and bulk samples. When the solid sample is thin or small, the excitation light will penetrate the sample and subsequently irradiate the solid sample holder. This interaction can affect the true photoluminescence signal of the sample. Therefore, the influence of the solid sample holder must be considered. Solid sample holders can sometimes be contaminated by the sample, producing a photoluminescence signal. To ensure the accuracy of the measurements, these holders must be thoroughly cleaned prior to use.

3.3.3. Laser secondary reflection light

In conventional time-resolved photoluminescence experiments employing pulsed excitation sources and detectors with temporal resolution (pulse width, timing jitter, or detector resolution) at the hundred-picosecond level or longer, secondary laser reflections typically introduce negligible distortion to the measured decay profiles. However, when employing femtosecond laser systems or detectors with time resolutions of several picoseconds or better, secondary reflections from rear surfaces of quartz plates or cuvette windows can induce additional sample excitation. This artifact leads to measurable distortions in the recorded decay kinetics, causing deviations from the sample's intrinsic photoluminescence behavior, as illustrated in Fig. 6.

When performing time-resolved photoluminescence experiments using femtosecond ultrafast spectrometer, an additional weaker peak is occasionally observed in the decay profile. To explore this phenomenon, we compared decay curves from two types of samples with different optical paths. In Fig. 6a, the thickness of the quartz substrate is about 1.5 mm. The time difference between the two peaks is about 10 ps, and the corresponding optical path difference is 3 mm (calculated from the speed of light). Similarly, in Fig. 6c, the thickness of the cuvette is about 12 mm. The time difference between the two peaks is about 80 ps, and the corresponding optical path difference is 24 mm (calculated from the speed of light). The time difference between the two peaks is proportional to the optical path of different types of samples.

For a solid sample based on a quartz substrate, as shown in Fig. 6a', the laser first irradiates the sample on the front surface of the quartz substrate (the sample thickness < 1 μm). At the same time, the laser passes through the sample and the quartz substrate to the rear surface of the quartz substrate, and then the laser penetrates the quartz substrate to the front surface after the secondary reflection of the laser on the rear surface of the quartz substrate, and resulting in the secondary excitation of the sample. The optical path difference between the primary and secondary excitations is about 3 mm, and the time difference is exactly about 10 ps according to the speed of light. This explains the dual-peak distortion in Fig. 6a.

For solution samples in cuvettes, as shown in Fig. 6c', the laser first irradiates the front surface of the cuvette, while the laser subsequently passes through the solution to the rear surface of the cuvette. Following secondary reflection from the rear surface, the laser re-enters the solution before reaching the front surface, leading to an approximately 24 mm optical path and an associated time difference of about 80 ps. This explains the dual-peak distortion in Fig. 6c. Therefore, these distortions are caused by the re-excitation of the sample, arising from the secondary reflection of the laser on the rear surface of the quartz substrate or cuvette. It is important to mention that for the solution samples in cuvettes, the time difference between the two peaks (corresponding the optical path difference), depends on the detector's focus position. In this study, the focus position is set at the cuvette's front surface.

By modifying the sample placement method (for the solid sample based on quartz substrate) and the laser incident angle, the re-excitation of the laser secondary reflection on the sample can be effectively reduced, and the time decay curve becomes normal, as shown in Fig. 6b and d. When the solid sample based on the quartz substrate is placed in reverse (that is, the sample is behind the quartz substrate), the laser irradiation on the front surface of the quartz substrate will not excite the sample, and the sample can only be excited to produce photoluminescence after the laser penetrates the quartz substrate to reach the

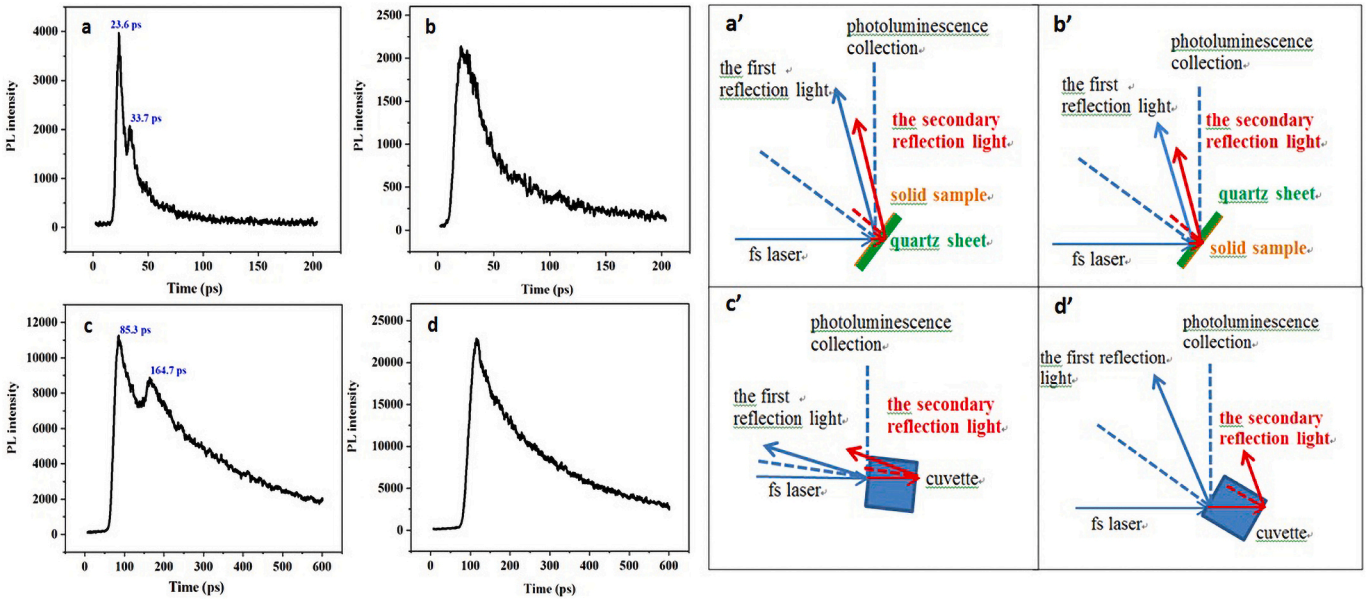

Fig. 6. Distortion of time-resolved photoluminescence decay curves due to the secondary laser reflections. **a, c** Distorted decay profiles corresponding to configurations **a'** and **c'**, exhibiting dual-peak structures with temporal separations of ~10 ps (**a**, thin film on quartz substrate) and ~ 80 ps (**c**, cuvette solution). **b, d** Normal decay profiles corresponding to configurations **b'** and **d'**, representing intrinsic sample emission.

sample, as shown in Fig. 6b'. For the cuvette solution sample, when the incident angle is about 30 degrees, the secondary reflected laser will not reach the front surface of the cuvette, and there will be no re-excitation of the sample, as shown in Fig. 6d'. This mechanism differs fundamentally from that reported in Reference [17]. In that work, the secondary signal was ascribed to the re-excitation of the sample by its own back-surface-reflected photoluminescence, which produced more intense up-converted luminescence than the primary excitation.

Furthermore, to exclude signal contamination (from either sample contamination or instrument artifacts) as the cause of the decay curve distortion, we performed an in-depth analysis. If impurities in the sample interact with the ground or excited states of the sample, or if the impurities themselves generate photoluminescence at the excitation wavelength, the decay rate of the excited state may be altered—either accelerated or decelerated—without introducing a second peak or distorting the decay curve shape. Furthermore, in cases where impurities are responsible, changing the angle between the laser and the sample will not affect the form of the decay curve, although it may influence the detected luminescence intensity. In addition, if the distortion originates from instrumental factors, adjustments such as varying the laser incidence angle or repositioning the solid sample will not alter the decay curve. Therefore, the observed distortion of the decay curve can be attributed to sample re-excitation caused by secondary reflection from the rear surface of optical components.

In summary, the generation of secondary reflection artifacts involves two main steps: (a) laser reflection from the rear surface of optical components (such as cuvette walls), and (b) re-excitation of the luminescent sample. In conventional photoluminescence spectrometers, the overall time resolution—limited by factors such as laser pulse width, timing jitter, and detector time response—is typically on the order of hundreds of picoseconds to nanoseconds. For solution samples in cuvettes or solid samples on quartz substrates, the time delay between the initial and secondary excitation is generally less than 100 ps. Since the time resolution of conventional spectrometers is insufficient to resolve such short delays, the resulting decay curve shows no discernible distortion from secondary excitation. In contrast, femtosecond ultrafast spectrometers (with a time resolution of ~2 ps) can readily detect these delays and secondary excitation of the sample often distorts the decay curve. Such distortions can usually be mitigated by adjusting the laser incident angle or modifying the placement of solid samples.

3.4. Experimental parameters

Various experimental parameters—including excitation energy density [21], excitation/emission slit dimensions, detector voltage (or gain setting), grating line density, pulse repetition rate, and photon counting frequency—can significantly influence photoluminescence measurements. While these conventional parameters are known to affect spectral data quality, the present study specifically examines two critical yet less explored factors: (1) laser pulse period and (2) peak photo count, with particular emphasis on their systematic effects on derived photoluminescence lifetime values.

3.4.1. Laser pulse period

The photoluminescence lifetime serves as a key parameter for probing the structural characteristics, microenvironment, and intermolecular interactions of luminescent materials. To obtain reliable lifetime values, it is essential to ensure complete decay of the photoluminescence decay curves. As demonstrated in Fig. 7a, we compare decay profiles acquired under different pulse periods (500 ns, 1000 ns, and 2000 ns), yielding fitted lifetime values of 38.8 ns, 38.8 ns, and 48.3 ns, respectively. Different pulse periods correspond to different pulse frequencies, and the pulse trigger delay is different, as shown in Fig. 7b, but the pulse trigger delay does not affect the fitted lifetime value. Rather, as shown in Fig. 7c, the pulse period emerges as the critical parameter affecting measurement accuracy.

For shorter pulse periods (500 ns and 1000 ns), the decay curve fails to fully attenuate and continues to decline monotonically. When the next pulse excites the sample, the photoluminescence produced by the previous pulse exciting sample has not yet been attenuated completely, and the photoluminescence photons arising from the previous pulse will accumulate in the next pulse cycle, resulting in the accumulation of photons in the frontal section of the next pulse cycle. Consequently, the derived lifetime value (38.8 ns for both cases) are artificially shortened due to this incomplete decay phenomenon. In contrast, the 2000 ns pulse period allows complete decay of the photoluminescence signal, enabling accurate determination of the true lifetime value (48.3 ns). This finding underscores the importance of selecting an appropriate pulse period that exceeds the characteristic decay time of the luminescent system by a sufficient margin to avoid photon accumulation artifacts.

3.4.2. Peak photo count

The photoluminescence lifetime value is theoretically independent of the peak photo count. However, for weakly luminescent samples, particularly when the peak photo count is very low (typically<500 photons), the decay curve may intersect the time axis prematurely. This phenomenon can lead to an artificially shortened photoluminescence lifetime value. When employing the time-correlated single photon counting (TCSPC) method, the number of photons at the peak is generally 3000–10,000. In this case, the derived photoluminescence lifetime value is closer to the intrinsic value, and the lifetime fitting value is more accurate. The dependence of the fluorescence lifetime of Rhodamine B on the peak photon count is presented in Supplementary Material.

Furthermore, critical consideration must be given to the photon accumulation time. Excessive accumulation durations may cause significant photodamage to photosensitive and thermosensitive samples, potentially altering their photophysical properties and compromising

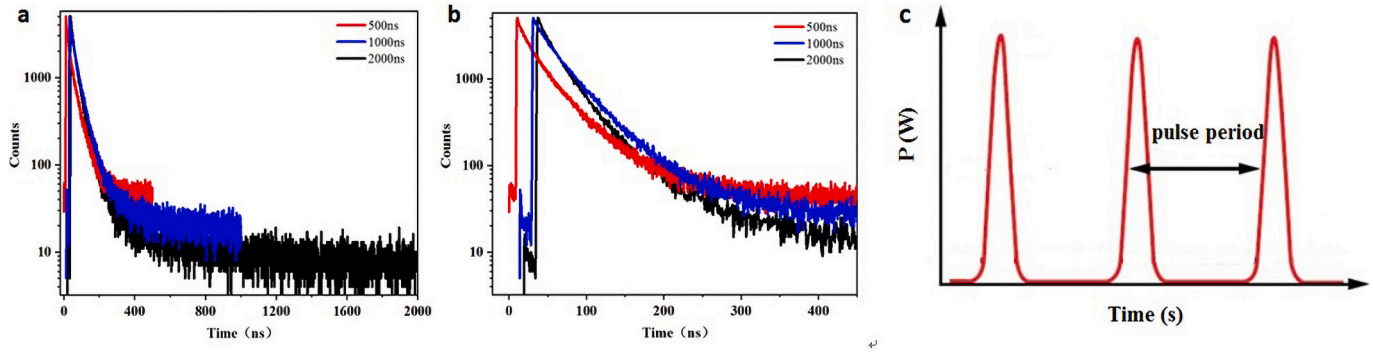

Fig. 7. a Photoluminescence decay profiles acquired under varying pulse periods (500 ns, 1000 ns, and 2000 ns). **b** Magnified view of decay curve regions. **c** Schematic representation of pulse period.

measurement validity. Therefore, a balance must be struck between obtaining adequate photon statistics and preserving sample property.

4. Conclusion

This study systematically examines critical factors affecting the reliability of photoluminescence measurements, encompassing both intrinsic instrument limitations and practical experimental limitations. Our investigation focuses on the complete optical pathway involved in photoluminescence generation, including light source characteristics, detector performance, monochromator efficiency, the interaction of the excitation light and sample, and key experimental parameters.

The wavelength-dependent variations in light source intensity, detector response, and optical component transmittance (gratings, collimating lenses) can be effectively corrected through proper calibration protocols. Instrumental limitations in grating performance, particularly for excitation wavelengths below 300 nm, generate stray light contamination in the 350–500 nm range, potentially producing spurious photoluminescence signals. This can be mitigated by optimizing excitation wavelength selection, adjusting slit widths at both excitation and emission ports and performing control experiments with instrument blanks. Strong sample scattering facilitates excitation light entry into the detector via grating higher-order diffraction, generating broadband stray light interference. Implementation of BP and LP filters significantly reduces these artifacts. When using ultrafast spectroscopy systems (time resolution $\leq$ tens of picoseconds), laser secondary reflections may distort decay profiles. These artifacts can be eliminated by modifying the laser incidence angle and inverting solid sample orientation. Quartz sample container are recommended over PTFE containers for more reliable quantum yield determinations. Complete decay curve attenuation is essential for accurate lifetime extraction. Insufficient peak photon counts ($<$500) may truncate the decay profile, artificially reducing the measured lifetime.

This work establishes a comprehensive framework for enhancing photoluminescence data reliability through identification of critical interference sources, development of effective mitigation strategies and provision of standardized methodologies for credible data acquisition. The presented solutions and practices will significantly improve the accuracy and reproducibility of photoluminescence measurements across various research applications.

Declaration of competing interest

The authors declare that they have no known competing financial interests or personal relationships that could have appeared to influence the work reported in this paper.

Acknowledgments

This work was supported by Chinese Academy of Sciences Key Technology Talent Program (Y929051R) and National Natural Science Foundation of China (E0A3032501). The authors thanks for the useful discussion about the grating performance with Zihao Xu at Huairou Research Center, Institute of Chemistry Chinese Academy of Sciences.

Appendix A. Supplementary data

Supplementary data to this article can be found online at https://doi.org/10.1016/j.saa.2025.127107.

Data availability

Data will be made available on request.

References

[1] GB/T 33252–2016 Nanotechnology-Performance testing for laser confocal microscope Raman spectrometers, issued on 2016-12-13 and implemented on 2017-07-1, 2025.
[2] N. Aizawa, Y.J. Pu, Y. Harabuchi, A. Nihonyanagi, R. Ibuka, H. Inuzuka, B. Dhara, Y. Koyama, K.I. Nakayama, S. Maeda, F. Araoka, D. Miyajima, Delayed photoluminescence from inverted singlet and triplet excited states, Nature 609 (2022) 502–516, https://doi.org/10.1038/s41586-022-05132-y.
[3] S. Sharma, R.D. Roppel, A.E. Murphy, L.W. Beegle, R. Bhartia, A. Steele, J.R. Hollis, S. Siljeström, F.M. McCubbin, et al., Diverse organic-mineral associations in Jezero crater, Mars. Nat. 619 (2023) 724–732, https://doi.org/10.1038/s41586-023-06143-z.
[4] C.F. Bohren, D.R. Huffman, Absorption and Scattering of Light by Small Particles, Wiley-Interscience, New York, 1998, p. 132.
[5] J. Harbinson, Improving the accuracy of chlorophyll fluorescence measurements, Plant Cell Environ. 36 (2013) 1751–1754, https://doi.org/10.1111/pce.12111.
[6] E. Bertone, A. Chuang, M.A. Burford, D.P. Hamilton, In-situ photoluminescence monitoring of cyanobacteria: laboratory-based quantification of species-specific measurement accuracy, Harmful Algae 87 (2019) 101625, https://doi.org/10.1016/j.hal.2019.101625.
[7] F.X. Sunahori, M. Gharaibeh, D.J. Clouthier, R. Tarroni, BH2 revisited: new, extensive measurements of laser-induced fluorescence transitions and ab initio calculations of near-spectroscopic accuracy, J. Chem. Phys. 12 (2015) 174302, https://doi.org/10.1063/1.4919094.
[8] L. Le Ster, H. Claustre, F. d'Ovidio, D. Nerini, B. Picard, C. Guinet, Improved accuracy and spatial resolution for bio-logging-derived chlorophyll a fluorescence measurements in the Southern Ocean, Front. Mar. Sci. 10 (2023) 1122822, https://doi.org/10.3389/fmars.2023.1122822.
[9] S.F. Silva, J.P. Domingues, A.M. Morgado, Can we use rapid lifetime determination for fast, fluorescencelifetime based, metabolic imaging? Precision and accuracy of double exponential decay measurements with low total counts, PLoS One 14 (2019) e0216894, https://doi.org/10.1371/journal.pone.0216894.
[10] Y. Kato, Y. Sakai, K. Sakai, K. Yasunobu, S. Yoshitsugu, Fluorescence intensity compensation method for accurately calculating intensity of fluorescence emitted from e.g. multiple fluorochromes excited by irradiating light on e.g. microparticles, involves obtaining measurement spectrum, Sony Corp., 2012. A43221, EP2405252 (A2, A3), EP2405252(B1).
[11] W. Jia, X. Zhang, Q. Shan, T. Chen, Y. Wang, H. Liu, Online potassium component detecting device, has sensor for monitoring fluctuation amount for distance compensation correction of fluorescence intensity, and combination mechanism for obtaining accuracy data of fluorescence measurement, Univ Nanjing Aeronautics & Astronautics (Unua-C), 2025. CN108693204-A, CN208366879-U, CN108693204-B, 2018-85012E.
[12] G. Li, F. Liu, F. Shao, J. Ma, Device for increasing accuracy and sensitivity of fluorescence optical fibre temperature measurement based on temperature sensor field, has capacitor whose end is connected with negative electrode of feedback resistance noise, Xian Optsensor Technology Co. Ltd., 2025. CN114878019-A, 2022-A5821T.
[13] Y.J. Won, W.T. Han, D.Y. Kim, Precision and accuracy of the analog mean-delay method for high-speed fluorescence lifetime measurement, J. Opt. Soc. Am. A Opt. Image Sci. Vis. 28 (2011) 2026–2032, https://doi.org/10.1364/JOSAA.28.002026.
[14] A.B. Thompson, E.M. Sevick-Muraca, Near-infrared fluorescence contrast-enhanced imaging with intensified charge-coupled device homodyne detection: measurement precision and accuracy, J. Biomed. Opt. 8 (2003) 111–120, https://doi.org/10.1117/1.1528205.
[15] J. C. Zwinkels, F. Gauthier, Instrumentation, standards, and procedures used at the National Research Council of Canada for high-accuracy fluorescence measurements. Anal. Chim. Acta 380 (1999)193–209, https:// doi.org/10.1016/S0003-2670(98)00603-5.
[16] D.R. Christmann, S.R. Crouch, A. Timnick, Precision and accuracy of absorption-corrected molecular fluorescence measurement by the cell shift method, Anal. Chem. 53 (1981) 2040–2044, https://doi.org/10.1021/ac00236a022.
[17] X.M. Wen, C. Lincoln, T.A. Smith, L.V. Dao, P. Hannaford, Characterization of the back surface reflection in InP using the femtosecond luminescence up-conversion, J. Phys. D. Appl. Phys. 42 (2009) 045115, https://doi.org/10.1088/0022-3727/42/4/045115.
[18] K.Y. Ji, Y.J. Xing, X.S. Niu, C.L. He, X. Dun, X.B. Cheng, Stray light analysis and suppression of broad-band spectral imaging system, Infrared and Laser Eng 52 (2023), https://doi.org/10.3788/IRLA20220645.
[19] Y.H. Li, C. Yang, C.X. Xue, X.T. Li, Z.Y. Ma, Stray light analysis and control of grating multistage diffraction in HRS, Acta Opt. Sin. 39 (2019) 0630001, https://doi.org/10.3788/AOS201939.0630001.
[20] J.C. de Mello, H.F. Wittmann, R.H. Friend, An improved experimental determination of external photoluminescence quantum efficiency, Adv. Mater. 9 (1997) 230–232, https://doi.org/10.1002/adma.19970090308.
[21] Y. Wan, A. Stradomska, S. Fong, Z. Guo, R.D. Schaller, G.P. Wiederrecht, J. Knoester, L.B. Huang, Exciton level structure and dynamics in tubular porphyrin aggregates, J. Phys. Chem. C 118 (2014) 24854–24865, https://doi.org/10.1021/jp507435a.